Laboratory similarity test relevant to salt cavern construction in interlayer-containing moulded saliferous aggregates specimen

De-Yi Jiang[1], Liang Yi[1,*], Jie Chen[1], Song Ren[1], Hua-Fu Qiu[2] and Yin-Ping Li[3]

[1]State Key Laboratory of Coal Mine Disaster Dynamics and Control, Chongqing University, Chongqing, 400030, China
[2]College of Energy Resource, Xian University of Science and Technology, Xian, 710054, China
[3]State Key Laboratory of Geomechanics and Geotechnical Engineering, Institute of Rock and Soil Mechanics, Chinese Academy of Sciences, Wuhan, 430071, China

Based on dimensional analysis, a similarity test relevant to salt cavern construction in interlayer-containing moulded saliferous aggregates was conducted. This moulded saliferous aggregates specimen can replace the drilling salt core for solution mining test. Experiments on the salt cavern construction adopting conventional single-well solution mining technology were performed in moulded saliferous aggregates specimen with two occurrence states: single-interlayer and double-interlayer. In the experiments, a method for determining the oil–water interface and cavern shape based on the conductive characteristics of saturated brine has been proposed. The experimental results illustrate that when the location of oil blanket is in the vicinity of the interlayer, the construction rate or leaching rate decreases because the interlayer reduces the effective dissolution area, and hinders the convection and diffusion of brine. Based on the adoptive dimensional analysis, the relationship between indoor model experiment and real-field salt cavern construction has been developed. Combining the results of indoor model experiments and numerical predictions using the simulation software SCB1.0, the capability of the new method to conduct solution mining process has been validated and could guide the field salt cavern construction.

Keywords: Dimensional analysis, saliferous aggregates, salt cavern, similarity test.

ACCORDING to statistical data of BP, one of the world's leading oil and gas companies, the worldwide natural gas consumption grew by 1.4% in 2013. The growth in China (+10.8%) and the US (+2.4%) was recorded as the most significant across the world, both accounting for 81% of the global consumption growth in 2013. Globally, natural gas accounts for 23.7% of primary energy consumption. The consumption of natural gas increased to 161.6 billion m^3 in 2013 in China. Because of the significant increase in natural gas consumption in China, the insufficient domestic gas production with 105.3 billion m^3 could not meet the country's requirements. This led to the dependency on natural gas imports from Russia and Turkmenistan via pipeline, and Austria via LNG ship[1].

Currently, there are five types of underground gas storage (UGS) facilities listed in the International Gas Union (IGU) database (2014) with a total storage of 358.8 billion m^3 of working gas. The main types are aquifer, gas field, oil field and salt cavern[2]. Salt cavern UGS accounts for merely 6% of the worldwide working gas volume (Figure 1). Despite the fact that gas field is the dominant storage method for natural gas, salt cavern storage has advantages related to higher deliverability, less cushion gas volume, less development cost, fast initiation of gas flow and quicker refill[3,4].

Most of the UGS in the world were constructed in geotechnically favourable domal salt formations in Germany, France, Denmark, Poland and US Gulf Coast areas. According to the growing demand for its flexible storage capacities, the construction of salt caverns in some less favourable salt formations became a trend in most countries, where ideal geotechnically suitable salt formations could not be found for salt cavern constructions[5–8]. China started a salt cavern UGS construction in Jintan, close to

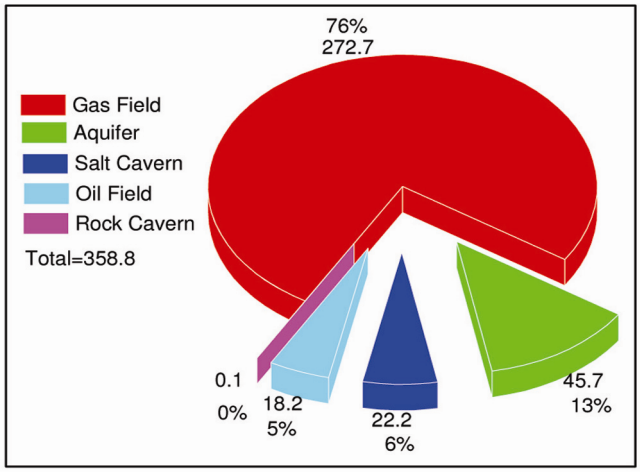

Figure 1. Working gas volume distribution by storage types (bcm).

*For correspondence. (e-mail: yiliangcqu@gmail.com)

Shanghai, to cover the energy shortage in the Yangzi Delta. The Jintan salt strata are almost horizontal and comprised of salt layers and intermediate mudstone layers. The gas is delivered from West China through the East-West Pipeline to the storage site. CNPC and Sinopec, two main oil and gas producers and suppliers in China, are constructing UGS in salt formations in YingCheng and Qianjiang in Hubei province, Huaian in Jiangsu province and Pingdingshan in Henan province[9–12].

Salt deposits in China generally contain many interlayers that are difficult to dissolve or are insoluble, such as anhydrite, glauberite and mudstone interlayers. In a cavern construction from the bottom up, the interlayers are gradually exposed in succession, which has a negative impact on cavern construction, such as breakage of the casing pipe and deformation in the cavern shape. Therefore, it is important to study solution mining features in bedded salt deposits[13–15].

Currently, the studies relevant to solution mining technology in bedded salt formation focus mainly upon mechanical properties[16], dissolution features[17,18], feasibility and stability analyses[19,20], and numerical methods[21,22]. There are few studies on indoor model test related to salt cavern construction in interlayer-containing moulded saliferous aggregates specimen. In this study, specimen with two different interlayer occurrence states – single-interlayer and double-interlayer was tested. The study has examined the variation of brine concentration, expansion tendency of cavern volume, cavern construction rate and the effect of interlayers.

Similarity theory

In the present study, a scale model was established based on dimensional analysis for studying the solution mining process in bedded salt deposits. The dimensional function for any physical quantity is always a power-law monomial, followed by a simple, naturally formulated principle. All systems with a given class are equivalent. Because of such advantage, dimensional analysis has been widely used[23,24].

The related parameters for cavern construction in salt deposits are as follows: geometric size (l), leaching time (t), density of the salt rock (ρ), dissolution rate (ω), concentration of the brine (c), temperature (T) and flow rate (q). The dimension of the parameters mentioned above in the LMT Θ class are:

$$[l] = L;\ [t] = T;\ [\rho] = ML^{-3};\ [\omega] = ML^{-2}\ T^{-1};$$

$$[c] = ML^{-3};\ [T] = \Theta;\ [q] = L^3T^{-1}.$$

There are four fundamental dimensions: L, M, T and Θ. L is the dimension of length; M the dimension of mass; T the dimension of time, and Θ is the dimension of temperature. According to the Π-theorem, there are three dimensionless quantities Π_1, Π_2, Π_3 in this system. l, t, ω and T were selected as the governing parameters with independent dimension, whereas the other three quantities were derived using the governing parameters. The parameter to be determined in this study is the flow rate, which can be expressed as follows

$$q = l^{\alpha} t^{\beta} \omega^{\lambda} T^{\gamma}. \tag{1}$$

According to the principle of dimensional homogeneity of the equation, $\alpha = 3$, $\beta = -1$, $\lambda = 0$ and $\gamma = 0$. Therefore, the dimensionless quantity Π_1, which is related to q, is expressed as follows

$$\Pi_1 = \frac{qt}{l^3}. \tag{2}$$

Similarly

$$\Pi_2 = \frac{\rho l}{t\omega}, \Pi_3 = \frac{lc}{t\omega}. \tag{3}$$

K represents the similarity ratio of the parameters. The geometric ratio can be expressed as follows

$$K_l = \frac{l_{\mathrm{p}}}{l_{\mathrm{m}}}, \tag{4}$$

where l_{p} represents the size of the prototype and l_m the size of the model. Similarly, $q_{\mathrm{p}}/q_{\mathrm{m}}$, $t_{\mathrm{p}}/t_{\mathrm{m}}$, $\omega_{\mathrm{p}}/\omega_{\mathrm{m}}$, and $c_{\mathrm{p}}/c_{\mathrm{m}}$ represent the ratios of the parameters of flow rate, leaching time, dissolution rate and concentration of brine q_{p}, t_{p}, ω_{p} and c_{p} in the prototype system to the corresponding parameters q_{m}, t_{m}, ω_{m} and c_{m} in the model system. Therefore, eqs (2) and (3) can be expressed as follows

$$\frac{K_{\mathrm{q}} K_{\mathrm{t}}}{K_l^3} = 1, \frac{K_{\rho} K_{\mathrm{l}}}{K_{\mathrm{t}} K_{\omega}} = 1, \frac{K_{\mathrm{l}} K_{\mathrm{c}}}{K_{\mathrm{t}} K_{\omega}} = 1. \tag{5}$$

Materials and methods

Materials

The test was conducted in interlayer-containing moulded saliferous aggregates specimen, but not drilling salt core[25]. This is because the drilling salt core specimens are easily damaged while coring and carrying, and the thickness and distribution of the interlayers in the specimens are hardly to be changed artificially. Moreover, the diameter of drilling salt cores is generally 100–150 mm, which cannot adequately characterize the solution mining process.

Natural salt powder from the Beibei area in Chongqing, China was used as the salt-bed material. The natural salt powder was screened and dried to remove large insoluble particles (Figure 2 *a*). These large insoluble particles were unevenly distributed in the interlayer-containing moulded saliferous aggregates specimen and could have an influence on the compactness of the moulded specimen. The existence of these large insoluble particles would have resulted in the perforation in the cavern in the subsequent laboratory model test. To achieve the required compactness of saliferous aggregates as the drilling salt core, the salt powder was dried at the temperature of 50°C. The particle size was less than 20 mesh, and the content of insoluble matter was 10%. Figure 2 *b* shows the treated salt powder.

Salt powder, cement, gypsum powder, sand and rosin were selected as components of the interlayer in the first specimen. However, in the second specimen, cement was not included as a component in the interlayer. The design seeks to examine two different types of interlayers, which differ in hardness. The interlayer with cement is considered hard and the one without cement is soft. A small quantity of rosin was used as the binder to bond the interlayer and salt bed. Tables 1 and 2 show the proportions of the components used.

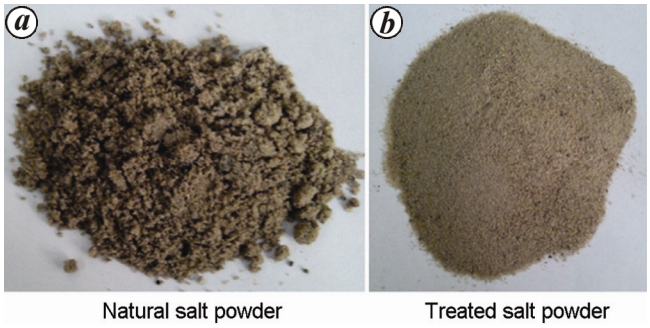

Figure 2. Natural and treated salt powder.

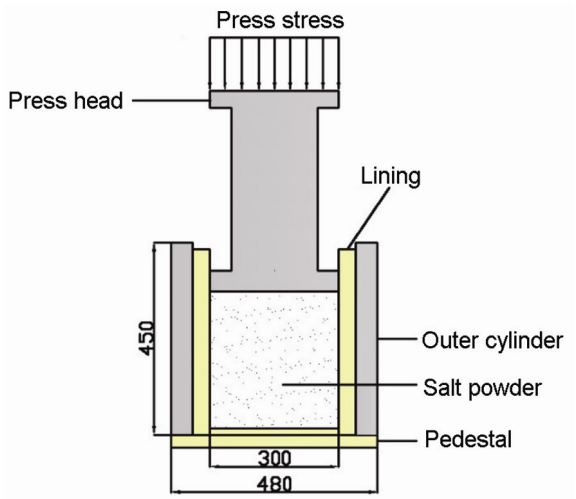

Figure 3. Press machine and mould for preparing large-sized interlayer-containing moulded saliferous aggregates specimen (mm).

Specimen preparation

Large-sized interlayer-containing moulded saliferous aggregates were obtained using a set of moulds. The moulds could be used to prepare specimen with a diameter of 300 mm and a maximum height of 500 mm. The compressive stress was set as 80 MPa and dwell time was 1 h (Figure 3).

Before production of the specimen, the mass of the salt layer and interlayer of the specimen needs be calculated based on density. The density of the large-sized specimen was the same as the small one. The density of the small, pure salt aggregates was 2.11 g/cm^3 and of the pure interlayer aggregates was 2.28 g/cm^3. This is similar to the density of Yun Ying salt core, with values of 2.3 g/cm^3 for pure salt rock and 2.65 g/cm^3 for the interlayers. The compactness of the moulded saliferous aggregates specimen could meet the requirement of solution mining test.

To study the solution mining process in bedded salt basin, two occurrence states of the interlayer were chose: single-interlayer and double-interlayer. For the single-interlayer, the thickness of the interlayer is 10 mm and is located at the centre of the specimen. For the double-interlayers, the thickness of each interlayer is 3 mm and the two interlayers are evenly distributed at the centre of the specimen. After the mass of interlayers and salt for each section were calculated, salt powder and interlayer materials were added into the mould accordingly. Because of the features of the selected press machine, the top of the prepared large-sized moulded saliferous aggregates specimen is relatively more compact. Therefore, there is an offset between the actual locations of the interlayer and the designated locations. The preparation process is as follows: (1) Prepare sufficient salt powder and interlayer materials required for the process. (2) Prepare the mould and evenly smear a release agent inside it. (3) Add the salt powder and interlayer materials into the mould accordingly. (4) Start the press machine, set the load at 80 MPa and maintain this load for 1 h.

Table 1. Composition of single interlayer

Components	Salt powder	Cement	Gypsum powder	Sand	Rosin
Percentage	20	30	25	20	5
Mass (g)	308	462	385	308	77

Table 2. Composition of double interlayer

Components	Salt powder	Sand	Gypsum powder	Rosin
Percentage	20	30	45	5
Mass (g)	59.2	88.8	133.2	14.8

(5) Then, clean the release agent off the surface of the specimen, measure the height of the moulded saliferous aggregates specimen, and determine the thickness and location of the interlayer.

Figure 4 shows the large-size interlayer-containing moulded saliferous aggregates specimens.

Experimental apparatus and operation methods

Experimental platform for cavern construction

The solution mining process in the interlayer-containing moulded saliferous aggregates specimen was completed in a self-fabricated experimental platform[26], which is shown in Figure 5. The circulation mode shown in the figure is reverse circulation. Freshwater was injected from the water tank, and the flow rate of freshwater was controlled by a flowmeter. The large-sized interlayer-containing moulded saliferous aggregates specimen was placed on the flat cart and covered by the steel drum. Paraffin was used to seal the annular space between the moulded specimen and steel drum to prevent against perforation and leakage during the cavern construction process.

Salinometer

During the experimental process, the concentration of brine was measured at the discharge outlet using a salinometer. The range of the salinometer was 0–28% (mass per centage concentration), with the minimum scale value of 0.2%.

Note that brine is measured as the mass–volume concentration in *in situ* cavern construction, whereas it is measured as the mass percentage concentration in the laboratory using a salinometer. The brine density establishes a relationship between these two concentrations. The density of different mass percentage concentrations of brine was, therefore, measured (Figure 6). The connection between density and mass percentage concentration of the brine was obtained by curve-fitting

$$\rho = 0.72\omega + 0.978. \tag{6}$$

The relationship between the mass–volume concentration and mass percentage concentration is

$$v = 1000 \cdot \rho \cdot \omega, \tag{7}$$

where v is the mass–volume concentration of brine, ρ the density of brine and ω is the mass percentage concentration of brine.

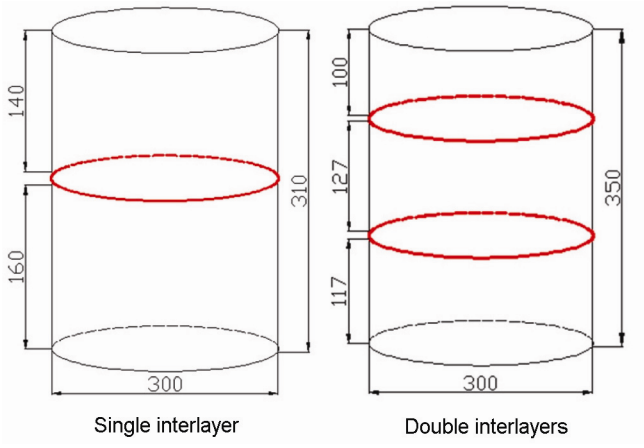

Figure 4. Large-sized interlayer-containing saliferous aggregates specimens (mm).

Cavern measuring instrument

The cavern measuring instrument consists a multimeter and a self-fabricated conducting rod, with a critical conducting location at the end of the rod (Figure 7). When the critical conducting location of the conducting rod touches the brine surface, the lines are connected. There is a change in the display of the multimeter, and the location of the brine surface is recorded. This method could be used to determine the designed location of the blanket medium during each period.

In an actual cavern construction process, it is necessary to use the sonar measurement for the cavern shape after each construction period. For laboratory experiments, it is not possible to use the sonar measurements for the small well-head; instead, the aforementioned cavern measuring instrument is used. If the cavern after each construction period is divided into N sections, then it consists of N thin disks. It is assumed that the distance between the location of a certain brine surface and the top of the cavern is H_k. After a certain volume (V_k) of saturated brine is added into the cavern, the distance between the brine surface in the cavern and top of the cavern changes to H_{k+1} and the radius (r) of the disk with its roof/floor H_k away from the top of the cavern is as follows

$$r = \sqrt{\frac{V_k}{\pi(H_k - H_{k+1})}}. \tag{8}$$

Different heights correspond to different radii, and the profile of the cavern can be obtained by connecting these points.

Experimental scheme

Determination of similarity ratios

In a solution mining process, the dissolution rate of the salt core is the key parameter which controls the

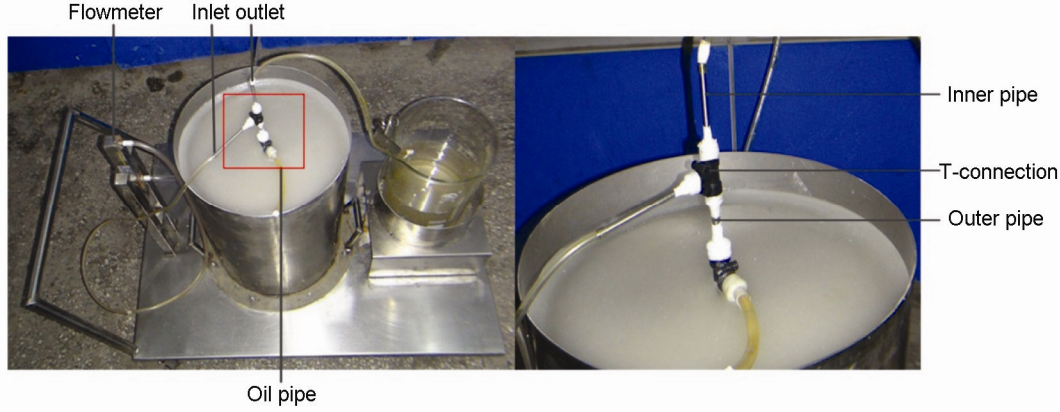

Figure 5. Experimental platform for cavern construction.

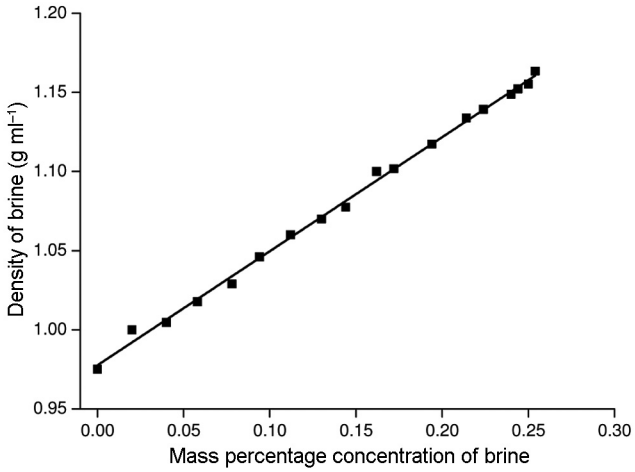

Figure 6. Relationship between density and mass percentage concentration of brine.

expansion of the salt cavern[27]. The dissolution rate of the large-sized specimen was hard to measure, so a small specimen was used for the dissolution experiment. The material of the small specimen and the large-sized specimen is the same; the small specimen was prepared under the same compressive stress. The small specimen was a cylindrical moulded saliferous aggregate with a diameter 50 mm and height 100 mm, and drilling salt core from the Yun Ying salt basin was used as the comparison specimen. The Yun Ying salt basin located in the northeastern Jiang Han plateau, Hubei province has a length of 33 km and width of 11 km (Figure 8). It covers an area of 260 sq. km, of which 188 sq. km forms the salt deposits. The salt reserves are estimated at 35.7 billion tonnes, with 25 billion tonnes of NaCl. The Yun Ying salt basin contains an Eocene evaporate at a depth between 300 and 850 m. The total thickness of the halite averages 30–90 m, and the thickest of the halite bed is approximately 180 m. Individual halite beds are several centimetres to 4.84 m thick and have relatively high purity with NaCl concentration of 75–85%. The interlayers are mainly made up of anhydrite and glauberite with insoluble concentration of 60–80%. The halite formation is overlaid and underlaid with anhydrite and glauberite. Table 3 shows the stratigraphic section of the Yun Ying salt basin.

The experiments were conducted at different temperatures, and at a dissolution angle of 90°. Dissolution occurred in freshwater. Table 4 lists the experimental results. According to the basic parameters of salt cavern in the Yun Ying salt basin, the depth of the cavern construction section is 300–850 m and the mean temperature in the cavern is 40°C. However, the experimental temperature was 20°C. From the values of the dissolution rates listed in Table 4, the similarity ratio of the dissolution rates could be obtained and used to deduce the similarity ratios of other parameters (Table 5).

Parameters of cavern construction

In this study, the construction of salt cavern in the bedded salt deposits has been simulated. The single-well solution mining technology that is often used in the field was adopted. To study the effect of different occurrence states of the interlayer on the salt cavern construction process, two sets of experiment were designed. Tables 6 and 7 list the parameters of the cavern construction. For the convenience of recording, the coordinate of the top surface of the moulded saliferous aggregates specimen was set as 0 mm, and the downward direction was set as positive. The drilling depths of the specimens were 280 and 300 mm respectively.

Results and discussion

Analysis of the concentration of brine

The concentration of brine at the discharge outlet was monitored during the cavern construction process. The concentration was observed to level-off as the cavern

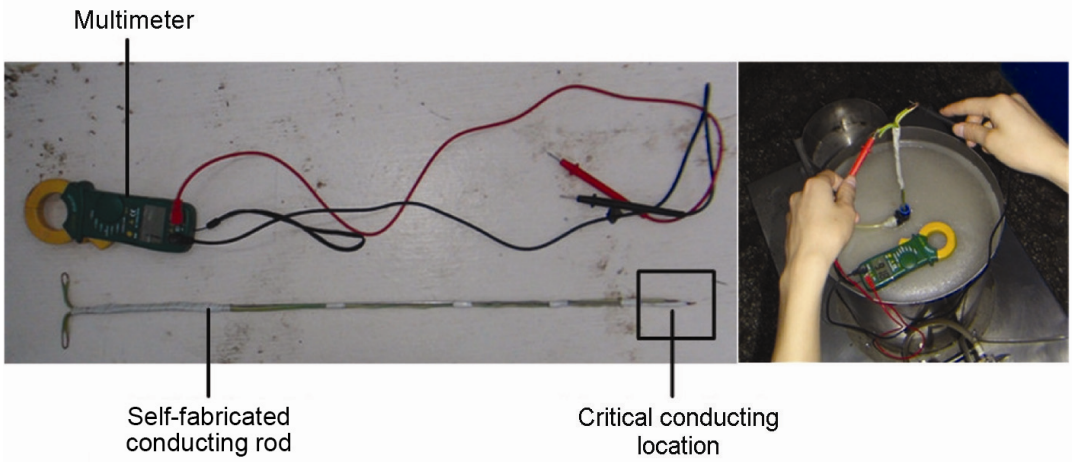

Figure 7. Cavern measuring instrument.

Table 3. Stratigraphic section of the Yun Ying salt basin

Age	Group	Code	Thickness (m)	Lithology
Quaternary		Q	11–153	Clay, sand and gravel
Tertiary	Wenfeng pagoda	E*w*	3–480	Lower: Celadon or ochre calcareous mudstone and siltstone. Upper: Light green, off white and ochre marlstone and siltstone.
	Gypsum-salt	E*g*	394–1598	Lower: Celadon silty mudstone, ochre sandy siltstone, and punctiform, crumby or laminated muddy anhydrite (Eg^1) Middle: Laminated with anhydrite, salt rock and glauberite. Upper: Interbedded glauberite (Eg^4), laminated with celadon anhydrite mudstone, muddy anhydrite and ochre siltstone (Eg^5).
	Bai Sha Kou	E*b*	694–920	Off white sandstone, siltstone and sandy mudstone
	Yuntai Mountain	E*y*	727	Fuchsia fine conglomerate, pebbly sandstone, sandstone, mudstone and shale.
Cretaceous	Gongan Zhai	K_2g	>350	Fuchsia inequigranular conglomerate, siltstone, mudstone and variegated shale

Table 4. Dissolution rate of moulded saliferous aggregates and drilling salt core under different temperatures

Specimen	Temperature (°C)	Dissolution rate (g cm^{-2} h^{-1})
Moulded saliferous aggregates	20	1.12
Moulded saliferous aggregates	25	1.22
Moulded saliferous aggregates	30	1.27
Moulded saliferous aggregates	35	1.43
Moulded saliferous aggregates	40	1.61
Drilling salt core	20	1.41
Drilling salt core	30	1.69
Drilling salt core	40	2.29

Table 5. Similarity ratio of parameters

Parameters	Prototype	Model	Similarity ratio
Radius (m)	30	0.1	300
Density (kg m^{-3})	2160	2110	1.02
Dissolution rate (g cm^{-2} h^{-1})	2.29	1.12	2.04
Time (h)	–	–	150
Concentration (g l^{-3})	–	–	1.02
Flow rate (ml min^{-1})	2.3×10^6	12.7	180,000

Figure 8. Location of Yun Ying salt basin in China.

construction progressed. However, the concentration slightly fluctuated during the levelling-off process in the first period. This was the result of the relatively small volume of the cavern in the initial construction period,

which was significantly affected by fluctuations of flow, thus causing the fluctuations of brine concentration inside the cavern. As shown in Figure 9, there was a relatively large fluctuation in the concentration during the sixth period, which resulted from leakages; thus, the cavern construction process had to be suspended. Construction resumed after the cavern had been repaired, but the brine concentration was significantly affected. The cavern construction process in the field, could also be suspended because of uncertain factors, such as circuit fault and vacuum pump fault.

During the cavern construction process in the large-sized single-interlayer-containing moulded saliferous aggregates specimen, the mean concentration of brine at discharge outlet exhibited a slight increment followed by concave-shaped trend with the progression of cavern construction (Figure 10). This phenomenon can be explained as follows: in the first cavern construction period, the circulation mode was normal, the volume of the cavern was small, and the effective area of dissolution was small; therefore, the overall concentration in the cavern was relatively low. In the second period, the circulation mode was reverse and the brine discharge outlet was located at the bottom of the cavern; thus, the concentration of brine increased significantly compared with that of the first period. With the continuous increase in the volume of the cavern, the concentration continued to increase, and the mean concentration reached 152 g/l^3 in the third period. In the fourth cavern construction period, the concentration decreased to some extent because the water inlet was located at the interlayer, whereas the location of the blanket medium was 1 cm above the interlayer. Thus, there was a decrease in the effective dissolution area, which resulted in a decrease in the concentration. In the fifth period, both the water inlet and blanket were located above the interlayer, and the interlayer did not collapse when immersed in brine. The interlayer hindered the initial flow of brine such that brine in the area below the interlayer was almost in a stationary state. Therefore, new cavern construction in the area above the interlayer started from the fifth period, and the concentration pattern increased again from the same period.

During the cavern construction process in the large-sized double-interlayer-containing moulded specimen, the concentrations were all relatively low from the first through fourth period because the circulation mode in the first, third and fourth periods was normal. Although the circulation mode in the second period was reverse, it was still at the initial cavern construction period, and the blanket was located on the bottom interlayer. Therefore, the concentration was relatively low. In the fifth and sixth periods, the cavern construction mode changed to reverse, and it was in the mid–late period. In addition, the effective area of dissolution was large; therefore, the concentration of brine in these two periods was above 230 g/l^3. In the last period of cavern construction, all of casing pipes were located above the top interlayer and construction was limited to a small area; therefore, there was a large reduction in the concentration of brine.

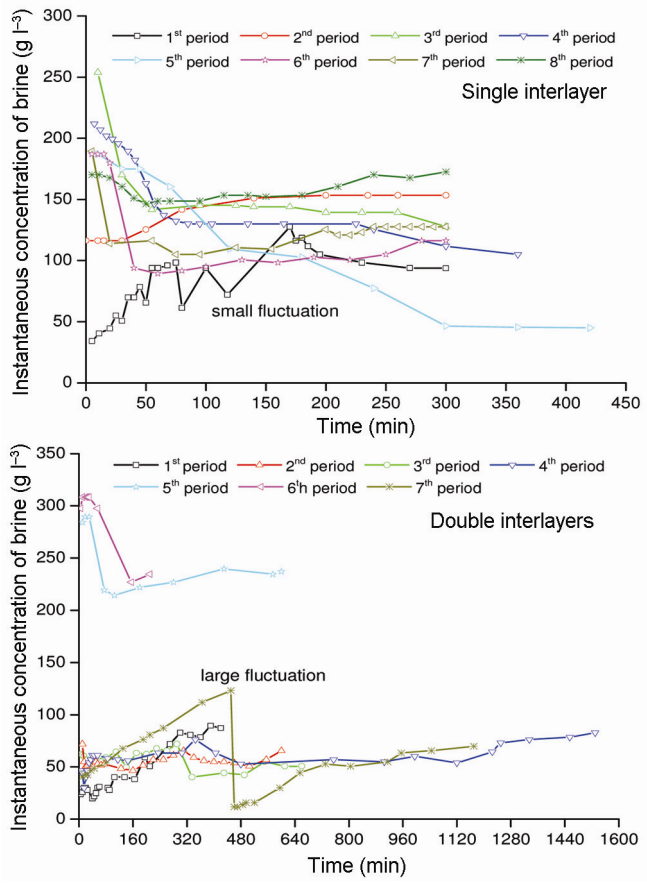

Figure 9. Instantaneous concentration of brine with time.

Analysis of the expansion of cavern volume

It is necessary to calculate the cavern volume during the cavern construction process. The volume of the dissolved

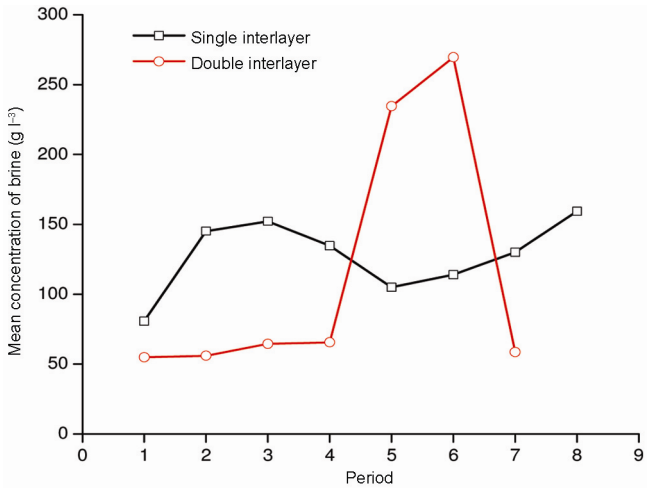

Figure 10. The varying pattern of mean construction of brine with period.

Table 6. Parameters of cavern construction in large-sized single-interlayer-containing moulded specimen

Period	Time (min)	Circulation model	Flow rate (ml/min)	Inner pipe (mm)	Outer pipe (mm)	Blanket (mm)
1	300	Normal	8	270	240	220
2	360	Reverse	12.7	250	210	190
3	300	Reverse	12.7	230	180	160
4	360	Reverse	12.7	210	150	130
5	420	Reverse	12.7	210	120	100
6	300	Reverse	12.7	180	90	70
7	300	Reverse	12.7	150	60	40
8	300	Reverse	12.7	150	30	10

Table 7. Parameters of cavern construction in large-sized double-interlayer-containing moulded specimen

Period	Time (min)	Circulation model	Flow rate (ml/min)	Inner pipe (mm)	Outer pipe (mm)	Blanket (mm)
1	420	Normal	12.7	290	270	250
2	600	Reverse	12.7	270	250	230
3	660	Normal	12.7	240	220	200
4	1530	Normal	12.7	220	190	170
5	600	Reverse	12.7	200	160	140
6	210	Reverse	12.7	180	130	110
7	1170	Reverse	12.7	100	70	50

salt rock (V) in the cavern in each period can be calculated by measuring the mass and mean mass percentage concentration of the discharged brine during each period. V can be expressed as

$$V = \frac{mc}{\rho(1-\varphi)},$$

where m is the mass of the discharged brine, c the mean mass percentage concentration of the discharged brine, ρ the density of the salt rock, and φ is the percentage of insoluble matter in the salt rock.

The cavern construction rate is defined as the cavern volume built per unit time. Figure 11 shows that the cavern construction rate in each period is consistent with the variation pattern of the mean concentration of the discharged brine. In addition, the turning point of the cavern construction rate is also the same as the turning point of the concentration of the discharged brine; and both these emerge when the expansion of the cavern reaches the vicinity of the interlayer. The final volume of the cavern constructed in the large-sized single-interlayer-containing moulded saliferous aggregates specimen was 2150 ml, and the final volume of the cavern calculated using eq. (9) was 2147 ml. The final volume of the cavern constructed in the large-sized double-interlayer-containing moulded saliferous aggregates specimen was 2400 ml, and the final volume of the cavern calculated using eq. (9) was 2481 ml. Thus, eq. (9) is reliable and can be used to estimate the volume of the cavern for each period.

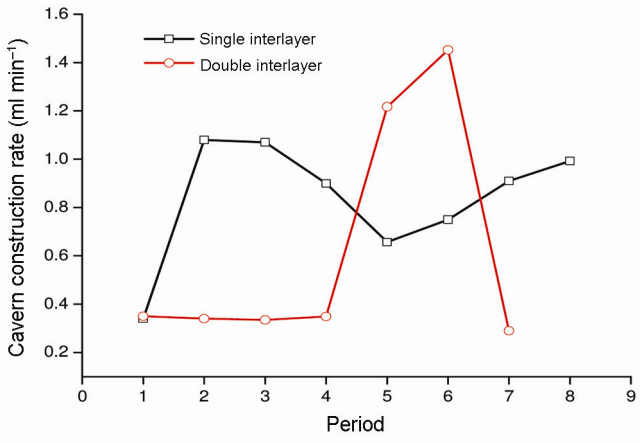

Figure 11. Construction rate of the cavern versus periods.

Analysis of cavern shape

The cavern shape measured using the cavern measurement method was similar to the actual constructed cavern shape, with the shapes basically overlapping each other; this validates the reliability of the cavern measurement method (Figures 12 and 13). The interlayer(s) divided the cavern into two or three small-scale caverns and thus reduced its capacity. The total height of the cavern constructed in the single-interlayer-containing moulded saliferous aggregates specimen was 257 mm, the maximum diameter of the top cavern was 200 mm, and the maximum diameter of the bottom cavern was 250 mm. The total height of the cavern constructed in the

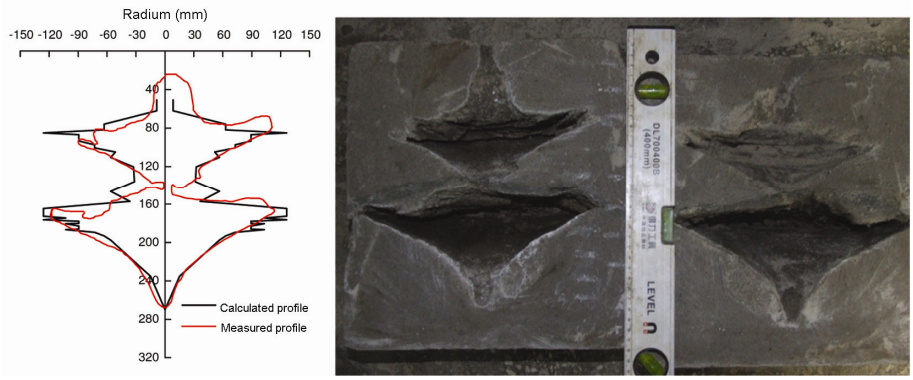

Figure 12. Profile of the cavern constructed in the single-interlayer-containing moulded saliferous aggregates specimen.

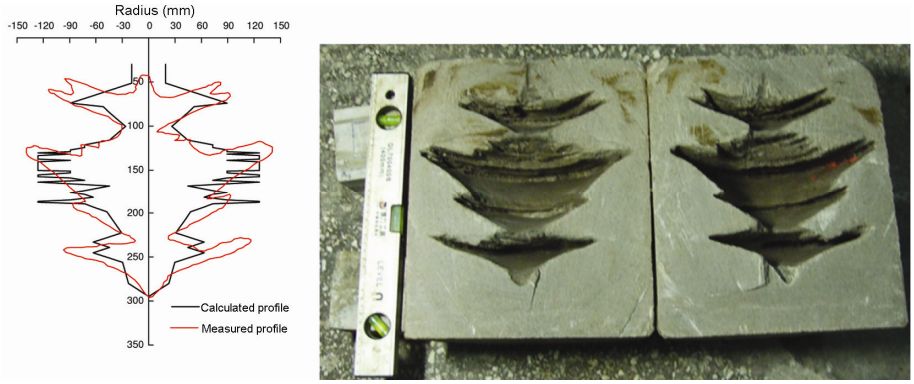

Figure 13. Profile of the cavern constructed in the double-interlayer-containing moulded saliferous aggregates specimen.

double-interlayer-containing moulded saliferous aggregates specimen was 250 mm, and the maximum diameter of the top, middle and bottom caverns was 190, 258 and 190 mm respectively.

Analysis of the capability of the new method

Based on the indoor similarity model experiment and similarity ratios listed in Table 5, the relationship between indoor cavern construction using large-sized interlayer-containing moulded saliferous aggregates specimen and field cavern construction can be established and used to derive the parameters of field cavern construction (Tables 8 and 9). The depth of the top surface of the single-interlayer-containing salt bed for field cavern construction was 520 m, and the thickness of the salt bed was set as 106 m. A height of 10 m was reserved for the top and 15 m for the bottom; thus, the height of the cavern construction was 81 m. The maximum diameter was 60 m, and the total leaching time required for cavern construction was 267 days. The cavern construction period and leaching time were converted according to a ratio of 85%. Thus, the period of cavern construction in the single-interlayer-containing salt bed was 314 days. The interlayer was located between 569 and 572 m depth, and the thickness of the interlayer was 3 m.

Based on the similarity ratios, the height of cavern constructed in the double-interlayer-containing salt bed was 75 m, maximum diameter was 60 m, flow rate was 137 m^3/h, total leaching time required for cavern construction was 542 days and total cavern construction period was 638 days. The cavern construction section was located between 530 and 605 m in depth, the top interlayer between 545 and 545.9 m, and the bottom interlayer between 584 and 584.9 m. The thickness of each interlayer was 0.9 m.

The capability of the new solution mining method was proven using the simulation software, Salt Cavern Builder V1.0 (SCB1.0), which for the cavern construction process in bedded salt deposits. SCB1.0 was developed based on Microsoft Visual C++ 6.0 (VC 6.0) and DirectX9.0, and it can be operated on mainstream Microsoft operation systems. Compared with other solution mining software, such as SMRI SALGAS Version 4.0 for Windows (Solution Mining Research Institute, USA) and UBRO (Chenkop, Warsaw, Poland), the advantage of SCB1.0 is that it can control the collapse of the inrelayers.

Salt cavern construction is a complex process of fluid dynamics and chemical kinetics. The basic principle of SCB1.0 is to establish a mathematical model that can describe the salt cavern construction process based on three-dimensional convection–diffusion dynamics as well

Table 8. Parameters of field cavern construction in the single-interlayer-containing salt bed

Period	Time (days)	Circulation model	Flow rate (m^3/h)	Inner pipe (m)	Outer pipe (m)	Blanket (m)
1	31	Normal	86	608	599	593
2	37	Reverse	137	602	590	584
3	31	Reverse	137	596	581	575
4	37	Reverse	137	590	572	566
5	44	Reverse	137	590	563	557
6	31	Reverse	137	581	554	548
7	31	Reverse	137	572	545	539
8	31	Reverse	137	572	536	530

Table 9. Parameters of field cavern construction in the double-interlayer-containing salt bed

Period	Time (days)	Circulation model	Flow rate (m^3/h)	Inner pipe (m)	Outer pipe (m)	Blanket (m)
1	44	Normal	137	602	596	590
2	63	Reverse	137	596	590	584
3	69	Normal	137	587	581	575
4	159	Normal	137	581	572	566
5	63	Reverse	137	575	563	557
6	22	Reverse	137	569	554	548
7	122	Reverse	137	545	536	530

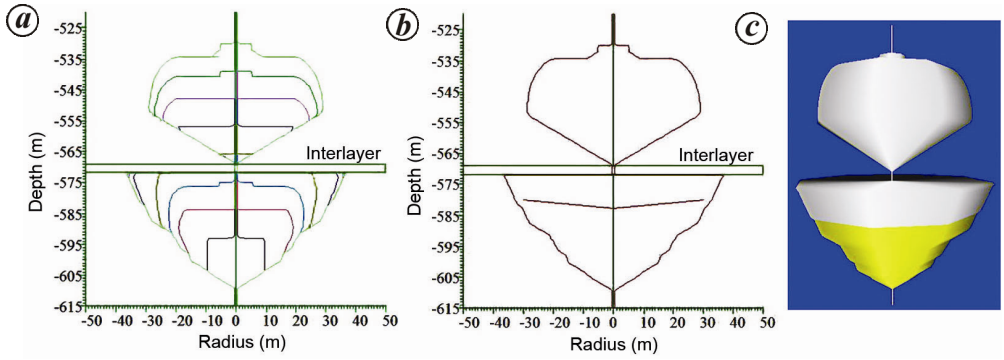

Figure 14. *a*–*c*, Profile of the cavern with single interlayer simulated by SCB1.0.

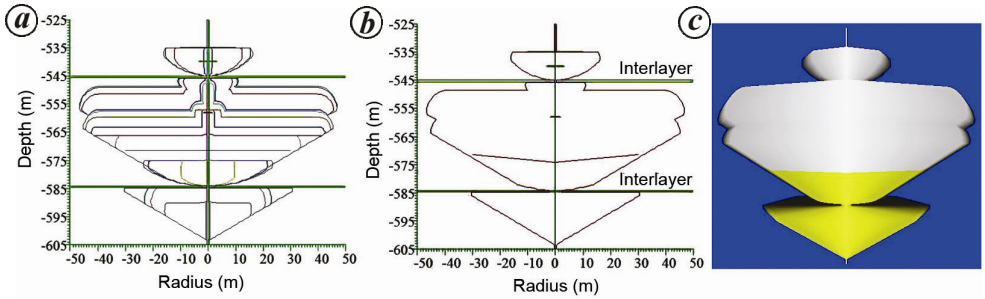

Figure 15 *a*–*c*. Profile of the cavern with double interlayer simulated by SCB1.0.

as fluid dynamics, chemical kinetics and thermokinetic theory. This mathematical model includes five sets of basic equations and balance equations of material exchange in normal and reverse circulations.

Based on the parameters listed in Table 8, the cavern construction process in a single-interlayer-containing salt deposit can be simulated. Figure 14 *a* shows the cavern expansion, Figure 14 *b* the two-dimensional map, and Figure 14 *c* the three-dimensional map of the cavern.

Based on the parameters listed in Table 9, the cavern construction process in a double-interlayer-containing salt deposit can be simulated. Figure 15 *a* shows the cavern expansion, Figure 15 *b* the two-dimensional map and Figure 15 *c* the three-dimensional map of the cavern.

The SCB1.0 simulation results were able to reproduce the effect of the interlayer on the cavern construction process. The profile of cavern that was simulated using SCB1.0 was close to the result obtained from the laboratory similarity experiment. Therefore, the simulated results could meet the engineering requirements, which indicates the practicality of using SCB1.0 and the feasibility of the new solution mining method discussed here.

Conclusion

In this study, an indoor model experiment was conducted in the interlayer-containing saliferous aggregates specimen, which was different from conventional leaching test carried out in the drilling salt core. This approach and its implementation were convenient and have the capability to solve the problems of non-optional crude salt core as test requirement, especially for bedded salt core. Based on dimensional analysis, the relationship between indoor model experiment and real-field construction was established, which provides a method to optimize the solution mining process. The numerical simulation software, SCB V1.0, could simulate solution mining process either in salt dome or bedded salt deposits. Combining the results of the indoor model experiment and numerical simulation, the applicability of the new method has been validated and could guide the field salt cavern construction.

1. BP Statistical Review of World Energy 2014; BP stats, www.bp.com/statisticalreview
2. Natural Gas Facts and Figures, IGU Resources and Data; www.igu.org/resources-data
3. Gillhaus, A., Natural gas storage in salt caverns–summary of worldwide projects and consequences of varying storage objectives and salt formation. In *Underground Storage of CO_2 and Energy* (eds Hou, M. Z., Xie, H. P. and Yoon, J. S.), CRC Press/Balkema, Leiden, The Netherlands, 2010, pp. 191–197.
4. Gillhaus, A., Crotogino, F. and Albes, S., Complication and evaluation of bedded salt deposits and bedded salt cavern characteristics important to successful cavern sealing and abandonment. In Research project report, Solution Mining Research Institute, Clark Summit, PA, USA, 2006.
5. Evans Jr, L. J., Istvan, J. A. and Mcdonald, D. T., Solution mining of caverns in the Salado bedded salt formation of West Texas for storage of natural gas. In SMRI 1994 Spring Meeting, Houston, Texas, 24–27 April 1994.
6. Evans Jr, L. J., Istvan, J. A. and Mcdonald, D. T., The effects of high insoluble content on the development of natural gas storage cavenrs in the bedded salt formation of West Texas. In 1997 Spring Meeting, SMRI Cracow, Poland, 11–14 May 1997.
7. Gillhaus, A., Natural gas storage in salt caverns – present status, developments and future trends in Europe. In SMRI 2007 Spring Conference, Basel, Switzerland, 29 April–2 May 2007.
8. Manocha, J. S., Solution mining and cavern storage in bedded salts of Ontario. In Solution Mining Research Institute 1993 Spring Meeting, Syracuse, New York, 26 April 1993.
9. Hou, M. Z., Gou, Y., Xie, L. and Zhang, R., Natural gas storage cavern design under special consideration of the thin bedded salt layer in Jintan and intermediate layers of mudstone. In *Underground Storage of CO_2 and Energy* (eds Hou, M. Z., Xie, H. P. and Yoon, J. S.), CRC press/Balkema, Leiden, The Netherlands, 2010, pp. 211–216.
10. Yang, C. H., Li, Y. P., Qian, Q. H., Wei, D. H., Chen, F. and Yin, X. Y., Feasibility study of using the existing solution – mined caverns in Jintan salt mine as gas storage. In *The Second Half Century of Rock Mechanics* (eds Olalla, C. *et al.*), Taylor and Francis, London, 2007, pp. 1241–1244.
11. Lin, Y. X., International technical cooperation in the solution mining technology of rock salt deposits in China. In SMRI Meeting, Dallas, Texas, 16–20 October 1988.
12. Lin, Y. X. and Nie, C. X., Technical development of solution mining in thinly bedded rock salt deposits of Ziliujing, Sichuan, China. In Sixth International Symposium on Salt, Toronto, Canada, 24–28 May 1983.
13. Yang, C. H. *et al.*, Feasibility analysis of using abandoned salt caverns for large-scale underground energy storage in China. *Appl. Energy*, 2015, **137**, 467–481.
14. Guo, Y. T., Yang, C. H. and Mao, H. J., Mechanical properties of Jintan mine rock salt under complex stress paths. *Int. J. Rock. Mech. Min.*, 2012, **56**, 54–61.
15. Li, Y. P., Shi, X. L., Yang, C. H. and Qu, D. A., Several key problems about control of solution mining for oil/gas storage in deep salt mine. *CJRME*, 2012, **31**(09), 1785–1796 (in Chinese).
16. Li, Y. P., Liu, W., Yang, C. H. and Daemen, J. J. K., Experimental investigation of mechanical behaviour of bedded rock salt containing inclined interlayer. *Int. J. Rock. Mech. Min.*, 2014, **69**, 39–49.
17. Durie, R. W. and Jessen, F. W., Mechanism of the dissolution of salt in the formation of underground salt cavities. *SPE J.*, 1964, **4**(2), 183–190.
18. Hovorka, S. D., Understanding the processes of salt dissolution and subsidence. In SMRI 2000 Fall Meeting, San Antonio, Texas, 15–18 October 2000.
19. Lord, A. S., Overview of geologic storage of natural gas with an emphasis on assessing the feasibility of storing hydrogen. Sandia Report, Sandia National Laboratory, Albuquerque, NM, 2009.
20. Bérest, P. and Brouard, B., Safety of salt caverns used for underground storage blow out; mechanical instability; seepages; cavern abandonment. *Oil Gas Sci. Technol.*, 2003, **58**(3), 361–384.
21. Edler, D., The status of modelling software for salt cavern leaching, identification of some unsolved problems and investigation of few of their aspects. In *Underground Storage of CO_2 and Energy* (ed. Hou, M. Z., Xie, H. P. and Yoon, J. S.), CRC Press/Balkema, Leiden, The Netherlands, 2010, pp. 173-180; 211–216.
22. Devries, K. L., Callahan, G. D. and Mellegard, K. D., Numerical simulation of natural gas storage caverns in bedded salt. In 40th US Symposium on Rock Mechanics, Anchorage, Alaska, 25–29 June 2005.
23. Barenblatt, G. L., Scaling, *Self-Similarity, and Intermediate Asymptotics: Dimensional Analysis and Intermediate Asymptotics*, Cambridge University Press, Cambridge, UK, 1996.
24. Langhaar, H. L., *Dimensional Analysis and Theory of Models*, Wiley, New York, 1951.
25. Wu, X. and Liu, C. W., Analysis of moulded coal porosity base on surface characteristics. *Procedia Eng.*, 2011, **26**, 1058–1064.
26. Picaut, J. and Simon, L., A scale model experiment for the study of sound propagation in urban areas. *Appl. Acoust.*, 2001, **62**(3), 327–340.
27. Guarascio, Martina and Musso, Solution mining development with single wells in a salt deposit with a high content of insoluble. In SMRI 1990 Fall Meeting, Paris, 14–19 October 1990.

ACKNOWLEDGEMENTS. We thank the National Natural Science Foundation of China (Grant No. 51304256), China Postdoctoral Science Foundation (Grant No. 2013M540620), the Fundamental Research Funds for the Central Universities (Grant No. 106112016CDJZR-245518), Chongqing University Postgraduates' Innovation Project and the Specialized Research Fund for the Doctoral Program of Higher Education of China (Grant No. 20130191130003) for providing financial support.

Received 24 June 2014; revised accepted 15 May 2015

doi: 10.18520/cs/v111/i1/157-167